Published in final edited form as:
Science. 2013 June 28; 340(6140): 1591–1594. doi:10.1126/science.1236425.

Deep Cortical Layers are Activated Directly by Thalamus

Christine M. Constantinople and **Randy M. Bruno***
Dept. of Neuroscience and Kavli Institute for Brain Science, Columbia University, New York, NY, USA

Abstract

The thalamocortical projection to layer 4 (L4) is thought to be the main route by which sensory organs communicate with cortex. Sensory information is believed to then propagate through the cortical column along the L4→L2/3→L5/6 pathway. We discovered that sensory-evoked responses of L5/6 neurons derive instead from direct thalamocortical synapses. Many L5/6 neurons exhibited sensory-evoked post-synaptic potentials with the same latencies as L4. Paired *in vivo* recordings from L5/6 neurons and thalamic neurons revealed significant convergence of direct thalamocortical synapses onto diverse types of infragranular neurons, particularly in L5B. Pharmacological inactivation of L4 had no effect on sensory-evoked synaptic input to L5/6 neurons. L4 is thus not an obligatory distribution hub for cortical activity, and thalamus activates two separate, independent "strata" of cortex in parallel.

The conventional model of neocortex is that sensory processing begins in L4, which has been known for a century to be the principal target of thalamic afferents. Cortical layers are believed to transform sensory information as excitation spreads serially along the L4→L2/3→L5/6 pathway (1–4). This hierarchical serial model is consistent with anatomical observations that axons of excitatory L4 neurons primarily innervate L2/3 and axons of L2/3 pyramidal neurons arborize extensively in L5/6 (1, 4). L5 neurons comprise a major output of the cortex, having the most substantial axonal innervation of subcortical and cortical structures, while L6 neurons transmit feedback to thalamus and cortex (4–6).

The same thalamocortical (TC) axons that arborize so extensively in L4 also have sparser branches in the infragranular layers at the L5–L6 border (7–11), which have been assumed to be modulatory (3, 11, 12). Recent quantitative measurements of reconstructed TC axons suggest, however, that innervation of L5/6 may be significant albeit less than that of L4 (8). Therefore, L5/6 neurons might integrate sensory information from at least two classes of inputs: the direct thalamocortical pathway and the indirect L4→L2/3→L5/6 pathway. We investigated this in adult rats administered local anesthetics and a sedative, which better approximate wakefulness than does general anesthesia (13, 14). We made *in vivo* whole-cell recordings from 176 neurons in barrel cortex and juxtasomal recordings from 76 neurons in ventral posterior medial (VPM) nucleus of thalamus, areas processing tactile input from the facial whiskers during environment exploration.

*To whom correspondence should be addressed: randybruno@columbia.edu.

The conventional model predicts that the responses of neurons in L5/6 should lag those in other layers. We compared the latencies of sensory-evoked sub- and supra-threshold responses of morphologically identified neurons in every layer of barrel cortex. Strong high-velocity whisker deflection evoked robust post-synaptic potentials (PSPs) in neurons in all cortical layers (Fig. 1A). L4 onset latencies preceded those in L2/3 (Fig. 1B, C; L4: 7.76 ± 0.16 ms, n = 24; L2/3: 11.04 ± 0.26 ms, n = 18; $p < 10^{-13}$). While the average L5 (9.44 ± 0.3, n = 53) and L6 latencies (10.68 ± 0.67 ms, n = 13) were longer than that of L4, many L5 cells rivaled L4 in latency. Moreover, the longer-latency PSPs among L5 cells occur simultaneously with, not after, the onsets of L2/3 cells (Fig. 1B, C). Many L5 cells exhibited spike latencies as short as cells in L4 (Fig. 1D–F).

Short L5/6 latencies could result from substantial thalamocortical convergence, which can be estimated from the probability of finding TC-L5/6 connections. Ideally, synaptic measurements are made *in vivo* rather than *in vitro* to avoid issues related to lack of background synaptic input, the concentrations of extracellular ions and neuromodulators, and severing of axons during slice preparation. We used a previously developed technique to identify and quantify individual synaptic connections in living animals (14). Whole-cell recordings were made from neurons in L5/6 during simultaneous juxtasomal recording of action potentials from somatotopically aligned VPM neurons (Fig. 2A, B). The average PSP (aPSP) that a single thalamic cell produces in a cortical neuron (Fig. 2C, D) was estimated by spike-triggered averaging and corrected for the contribution of unrecorded inputs (see SOM).

Monosynaptic connections were observed onto L5/6 neurons (10 of 55 topographically aligned pairs tested, including morphologically identified and unidentified cells). Of the morphologically identified subset (Fig. 2E), connections were observed more frequently onto L5 pyramidal neurons (26%, 7 connected of 27 pairs tested) than onto L6 cells (9%, 1 of 11). Connections were not observed onto topographically unaligned cells or pyramidal neurons with apical trunks extending through the septal region between L4 barrels (Fig. 2E).

Individual TC connections onto infragranular neurons produced relatively small depolarizations (mean ± SD 571 ± 46.5 μV, median 463 μV, range 137 μV to 1.18 mV; Fig. 2F), similar to TC-L4 synapses (~500 μV; (14)). Mean onset latencies and 20–80% rise times were 2.40 ± 0.31 and 6.17 ± 4.55 ms, respectively. Neurons in each layer responded to conventional high-velocity stimuli with PSPs proportional to the probability of finding TC connections in that layer (Fig. 2G), consistent with direct TC connections producing sensory-evoked responses.

Morphological and physiological subtypes, which correlate with spatially intermingled L5/6 neuronal subclasses having distinct project targets (15, 16), may be preferentially thalamorecipient (9). Monosynaptic TC connections were observed most frequently on L5 thick-tufted neurons (44%, 4 connected of 9 pairs tested) but were also observed on L5 thin-tufted (17%, 3 of 18) and L6 (9%, 1 of 11) pyramidal neurons (Fig. 2H, I; Fig. S1A) and smooth interneurons (1 of 3). *In vitro* L5 thick-tufted neurons are typically “intrinsically bursting” (IB) whereas adapting trains of single spikes are more typical of the “regular-spiking” (RS) L5 thin-tufted neurons (9, 16). The predominant firing type of both

morphological classes *in vivo*, however, was IB (Fig. S1B, C), possibly due to our awake-like conditions, and monosynaptic connections were observed onto both physiological cell types (Fig. S1D, E). By contrast, most connected cells had somata at depths of 1400–1600 μm, where thalamic axons arborize in L5B/6A (7, 8), even though we sampled substantially from depths shallower than 1400 μm (Fig. 2J, left). Neurons in the TC arborization zone near L5B had the largest sensory-evoked PSPs (Fig. 2J, right).

Given that a whisker's representation in VPM contains ~200 neurons (14), 9–44% convergence is substantial, translating into ~20–90 thalamic connections per cell depending on its type. While individual TC synapses are weak, this number of synchronous convergent inputs may provide a second powerful pathway into the cortex, capable of directly driving the activity of L5 and responsive L6 cells. We therefore sought to dissect the contributions of the direct TC pathway and the indirect L4→L2/3→L5/6 pathway to the sensory responses of infragranular neurons, by inactivating L4 during sensory stimulation. Silencing of L4 was achieved by pressure ejection of lidocaine and confirmed by monitoring the local field potential (LFP) through the drug pipette. Beyond blocking action potentials in L4 cells, lidocaine suppresses axonal conduction within L4, along TC axonal branches that extend directly into L3, and along the radial trunk axons from L2/3 cells that traverse L4 to synapse in L5/6. This manipulation thus disconnects the upper and lower cortical layers, leaving intact the TC-L5/6 pathway.

To validate our manipulation, we performed whole-cell recordings of L4 neurons located 150 μm from the LFP/drug pipette (Fig. 3A). Lidocaine injection not only prevented these L4 cells on the other side of the barrel from discharging any action potentials, but also robustly and reliably eliminated virtually all spontaneous and sensory-evoked synaptic input (Fig. 3B–D; n = 6, from 10.71 ± 1.21 to 0.27 ± 0.08 mV, p = 0.0004). Given the high connectivity among L4 barrel neurons (p(connection) ~ 0.3; (4)), this dramatic reduction in synaptic input confirms that our manipulation silenced virtually all neurons in a barrel. Replacing the whole-cell pipette with an LFP pipette yielded similar results (Fig. S2A–C), further demonstrating that lidocaine inactivated a diameter exceeding 300 μm, more than the size of a barrel (~200–300 μm wide). Additionally, L4 inactivation reduced L2/3 synaptic inputs and prevented L2/3 spiking (Fig. S2D–F).

We then recorded synaptic inputs from morphologically identified neurons in L5/6 while inactivating the overlying L4 barrel (Fig. 3E). L5/6 pyramidal neurons deeper than 1350 μm from the pia were targeted to avoid direct drug effects on recorded cells and to sample the region of highest thalamocortical connectivity (Fig. 2J). Despite reducing the amplitude of the sensory-evoked LFP in L4 (n = 12; from 0.69 ± 0.09 to 0.21 ± 0.03 mV, p = 0.0001), lidocaine had virtually no effect on the sensory-evoked synaptic inputs of L5/6 neurons (Fig. 3F–G), in terms of amplitude (from 7.53 ± 0.98 to 7.58 ± 0.75 mV, p = 0.93; Fig. 3H) or onset latency (Fig. S3A, B). Mean and variance of spontaneous membrane potential fluctuations were similarly unaffected (Fig. S3B).

Even after L4 inactivation, sensory stimuli continued to evoke L5/6 action potentials (Fig. 3I, J; 0.16 ± 0.07 versus 0.12 ± 0.04 spikes/stimulus, p = 0.64). While L5/6 spiking was unaffected on average, some individual neurons appeared to increase/decrease their firing

rates (Fig. 3J). To test whether this was simply due to spiking variability, L5/6 spiking during “test” and subsequent “re-test” periods were compared. Individual L5/6 cells exhibited a range of firing rate differences between the test and re-test periods similar to the pre- and post-lidocaine periods (Fig. S3C).

How can thalamus effectively elicit L5 spikes given that L5 receives less thalamocortical convergence and exhibits smaller PSPs than L4? The mean spontaneous membrane potential of each L5 neuron was significantly closer to its spike threshold, compared to neurons in L4 and L6 (Fig. 3K), and distance to threshold correlated with responsiveness (Fig. S3E). Therefore, the relative depolarization of L5 cells here enables less synaptic input than available to L4 to become suprathreshold in 53% of cells (Fig. S3F, G). In contrast the smaller sensory-evoked PSPs and relative hyperpolarization of L6 (Fig. 2G, 3K) render 81% of its cells silent (Fig. S3F, G), consistent with L6 corticothalamic cells being unresponsive to sensory stimulation (see 6).

Muscimol injection to inactivate VPM neurons but spare fibers of passage substantially reduced PSPs of aligned L5/6 neurons (Fig. S4A, B). Residual PSP did not derive from neighboring cortical columns (Fig. S4C, D). A likely source is the secondary thalamic area, the posterior medial (POm) nucleus which arborizes in L1 and L5A, consistent with some L5 cells receiving mixed VPM and POm input (17). We tested whether long-range inputs, including axons from POm, S2, M1, and the callosum, contribute to L5 sensory responses via synapses onto apical tufts in L1. Pial application of lidocaine blocks L1 synapses, indicated by its ability to silence L2 (Fig. S5A–C). L5 PSPs were unaffected by combined L1/L4 inactivation (Fig. S5D, E). If ascending pathways such as those from POm contribute to deep layer sensory responses, it is likely via axon collaterals in L5/6 rather than in L1.

Our study demonstrates that primary thalamic nuclei, like VPM, can simultaneously copy the same signals to L4 and L5B, where they are processed in parallel (Fig. 4B) instead of serially through L4 (Fig. 4A). The TC→L4→L2/3 pathway and the TC→L5/6 pathway appear independent with regard to ascending sensory signals. TC axons innervate both middle and deep layers in multiple species (human, monkey, rat, and cat) and neocortical systems (motor, visual, auditory, and somatosensory) (18–22). Tuning of extracellular units in infragranular layers of cat visual and rodent somatosensory cortex often persists following lesion of L2/3 (23, 24), and some such units respond as early as middle layers (25, 26). Direct thalamocortical engagement of infragranular neurons may therefore be a general feature of neocortex.

Neocortical columns may contain two separate processing systems or “strata”: an upper stratum (L4 and L2/3) and a lower stratum (L5/6) possibly subserving different functions. This architecture may elaborate receptive fields via intralaminar cross-columnar rather than interlaminar connections. Moreover, L2/3 targets other neocortical regions whereas L5/6 targets both cortical and subcortical structures. While some subcortical projections provide feedback (i.e., to brainstem and primary thalamic nuclei), many of the subcortical targets, especially those of L5, are action-related (striatum and spinal cord) or high-order (secondary thalamic nuclei, which innervate high-order cortical regions). Both strata therefore have direct access to the same sensory information and can alter behavior via different anatomical

pathways. Consistent with the idea of two distinct systems, fate mapping studies recently demonstrated that the upper and lower strata develop from two distinct populations of radial glial cells (27).

Our results further demonstrate that propagation of excitation cannot be inferred solely from synaptic strength or axonal sparsity/density. L2/3's extremely low firing rates (13, 28–30) may explain its minimal contribution to sensory signals in deep layers, which by contrast are highly active. The activity and interactions of the layers may be behaviorally gated by comparisons of motor, state, and sensory signals (6, 31, 32) or by induction of learning.

Supplementary Material

Refer to Web version on PubMed Central for supplementary material.

Acknowledgments

We thank Larry Abbott, Richard Axel, Attila Losonczy and Ken Miller for manuscript comments, Drew Baughman for technical support, and Marissa Ilardi for morphological reconstruction. Support: NINDS NS069679, Rita Allen Foundation, Klingenstein Fund, and NSF Student Fellowship.

REFERENCES AND NOTES

1. Gilbert CD, Wiesel TN. Nature. 1979; 280:120. [PubMed: 552600]
2. Douglas RJ, Martin KA. Annu Rev Neurosci. 2004; 27:419. [PubMed: 15217339]
3. Callaway EM. Neural Netw. 2004; 17:625. [PubMed: 15288888]
4. Feldmeyer D. Front Neuroanat. 2012; 6:24. [PubMed: 22798946]
5. Oberlaender M, et al. Proc Natl Acad Sci U S A. 2011; 108:4188. [PubMed: 21368112]
6. Lee S, Carvell GE, Simons DJ. Nat Neurosci. 2008; 11:1430. [PubMed: 19011625]
7. Wimmer VC, Bruno RM, de Kock CP, Kuner T, Sakmann B. Cereb Cortex. 2010; 20:2265. [PubMed: 20453248]
8. Oberlaender M, Ramirez A, Bruno RM. Neuron. 2012; 74:648. [PubMed: 22632723]
9. Agmon A, Connors BW. J Neurosci. 1992; 12:319. [PubMed: 1729440]
10. Beierlein M, Connors BW. J Neurophysiol. 2002; 88:1924. [PubMed: 12364518]
11. Viaene AN, Petrof I, Sherman SM. J Neurosci. 2011; 31:12738. [PubMed: 21900553]
12. Guillery RW, Sherman SM. Neuron. 2002; 33:163. [PubMed: 11804565]
13. Constantinople CM, Bruno RM. Neuron. 2011; 69:1061. [PubMed: 21435553]
14. Bruno RM, Sakmann B. Science. 2006; 312:1622. [PubMed: 16778049]
15. Chagnac-Amitai Y, Luhmann HJ, Prince DA. J Comp Neurol. 1990; 296:598. [PubMed: 2358553]
16. Hattox AM, Nelson SB. J Neurophysiol. 2007; 98:3330. [PubMed: 17898147]
17. Bureau I, von Saint Paul F, Svoboda K. PLoS Biol. 2006; 4:e382. [PubMed: 17121453]
18. Ferster D, LeVay S. J Comp Neurol. 1978; 182:923. [PubMed: 103938]
19. Blasdel GG, Lund JS. J Neurosci. 1983; 3:1389. [PubMed: 6864254]
20. Herkenham M. Science. 1980; 207:532. [PubMed: 7352263]
21. Huang CL, Winer JA. J Comp Neurol. 2000; 427:302. [PubMed: 11054695]
22. Garcia-Marin V, Ahmed TH, Afzal YC, Hawken MJ. J Comp Neurol. 2013; 521:130. [PubMed: 22684983]
23. Schwark HD, Malpeli JG, Weyand TG, Lee C. J Neurophysiol. 1986; 56:1074. [PubMed: 3783230]
24. Huang W, Armstrong-James M, Rema V, Diamond ME, Ebner FF. J Neurophysiol. 1998; 80:3261. [PubMed: 9862920]

25. de Kock CP, Bruno RM, Spors H, Sakmann B. J Physiol. 2007; 581:139. [PubMed: 17317752]
26. Maunsell JH, Gibson JR. J Neurophysiol. 1992; 68:1332. [PubMed: 1432087]
27. Franco SJ, et al. Science. 2012; 337:746. [PubMed: 22879516]
28. O'Connor DH, Peron SP, Huber D, Svoboda K. Neuron. 2010; 67:1048. [PubMed: 20869600]
29. Hromadka T, Deweese MR, Zador AM. PLoS biology. 2008; 6:e16. [PubMed: 18232737]
30. de Kock CP, Sakmann B. Proc Natl Acad Sci U S A. 2009; 106:16446. [PubMed: 19805318]
31. Niell CM, Stryker MP. Neuron. 2010; 65:472. [PubMed: 20188652]
32. Keller GB, Bonhoeffer T, Hubener M. Neuron. 2012; 74:809. [PubMed: 22681686]

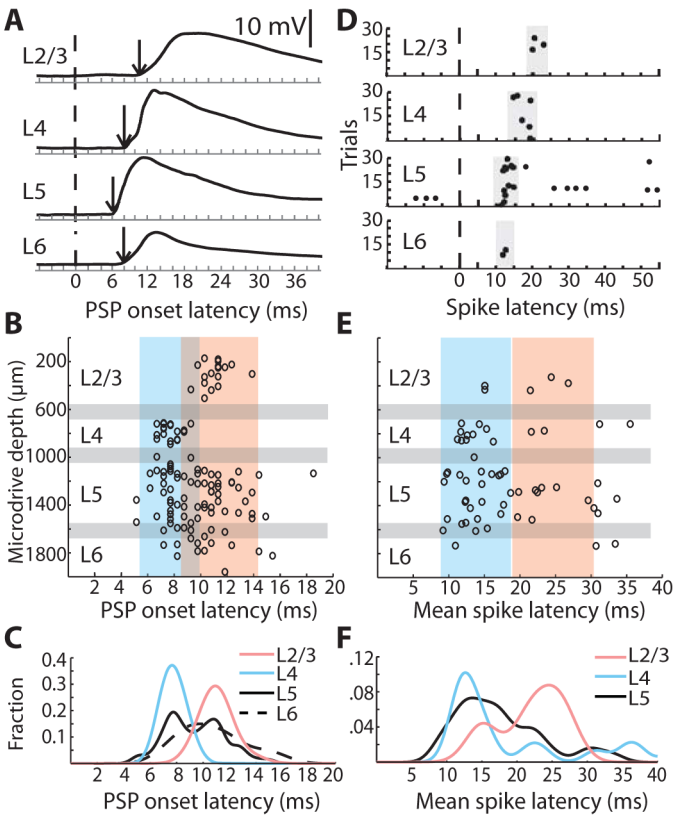

Fig. 1. Many L5/6 cells have response latencies as short as L4

(**A**) Example whole-cell traces from histologically identified cells. Dashed line, time of whisker deflection; arrow, PSP onset. (**B**) PSP onset latencies by microdrive depth (n = 126). Gray bars, approximate laminar boundaries correspond to the microdrive depths where histologically recovered neurons were found in each layer. Blue and pink boxes, approximate extent of the densities of L4 and L2/3 data, respectively, as in panel **C**. (**C**) Normalized probability densities of PSP onset latencies. (**D**) Example raster plots of cells in each layer relative to whisker deflection. (**E**) Distribution of mean spike latencies for responsive cells (n = 64) by microdrive depth. (**F**) Normalized probability densities of mean spike latencies. L6 density was not calculated due to insufficient spiking.

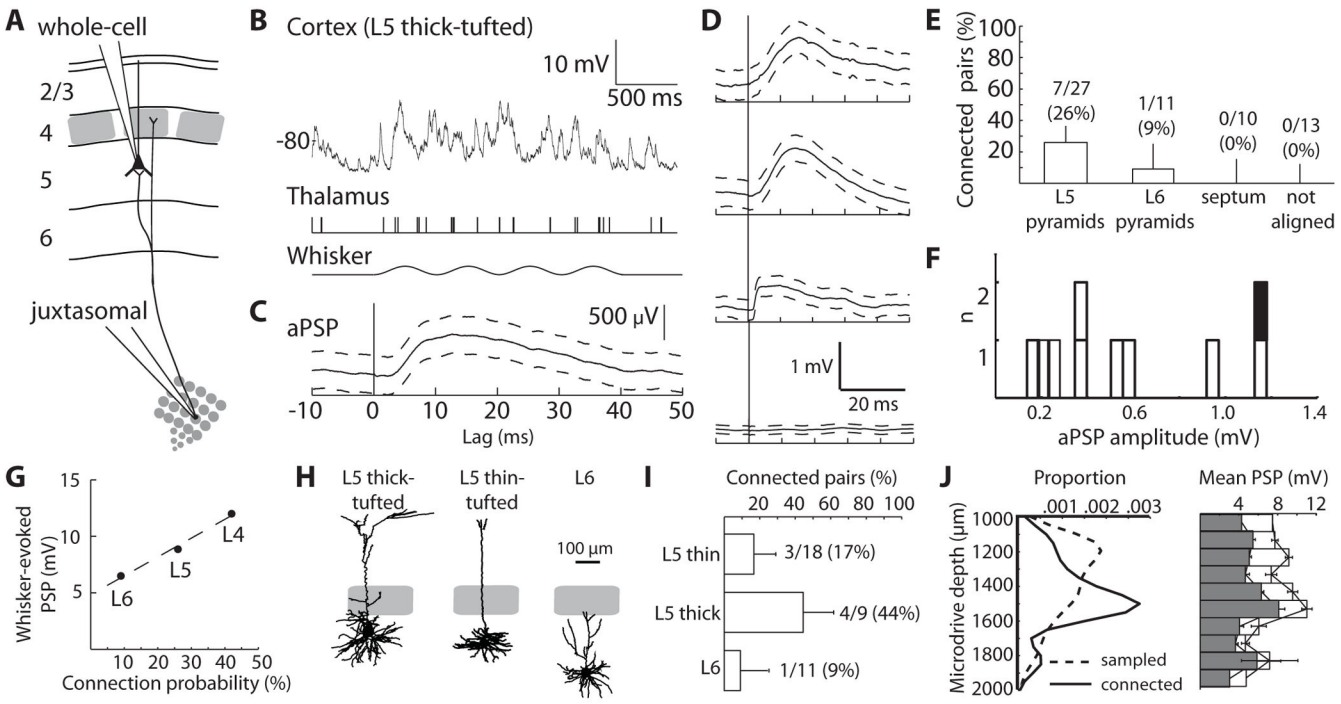

Fig. 2. TC connections onto infragranular neurons are weak but convergent

(**A**) Schematic of simultaneous *in vivo* whole-cell recording of a cortical L5 pyramidal neuron and extracellular recording of a somatotopically aligned thalamic neuron. (**B**) Example whole-cell trace from a L5 thick-tufted cell (top), action potentials from a thalamic neuron (middle), and sinusoidal whisker stimulus (bottom). (**C**) The aPSP measured from the above pair (n = 1076 thalamic action potentials). Dashed lines, 95% confidence intervals. (**D**) Example aPSPs onto L5 thin-tufted, L6, and L5 thick-tufted pyramidal neurons and example unconnected pair (from top to bottom). (**E**) Percentage of connected pairs by cortical cell location. Error bars, 95% confidence intervals for a binomial distribution. (**F**) Distribution of aPSP amplitudes. Black, smooth interneuron. (**G**) Amplitude of mean sensory-evoked PSPs (10–20 deflections in the preferred direction) for L4, L5 and L6 cells (n = 40, 35 and 11) versus probability of finding connected pairs in each layer. Dashed line, least-squares fit. L4 data are from ref (14). (**H**) Example reconstructions. (**I**) Connection probability by morphological subtype. (**J**) (Left) Densities of the depths of all sampled cells (dashed line) and cells onto which TC connections were observed (solid line). (Right) Mean sensory-evoked PSP amplitude by depth (mean +/− SEM; 100 µm bins). Open bars, preferred direction. Filled bars, average over 8 directions.

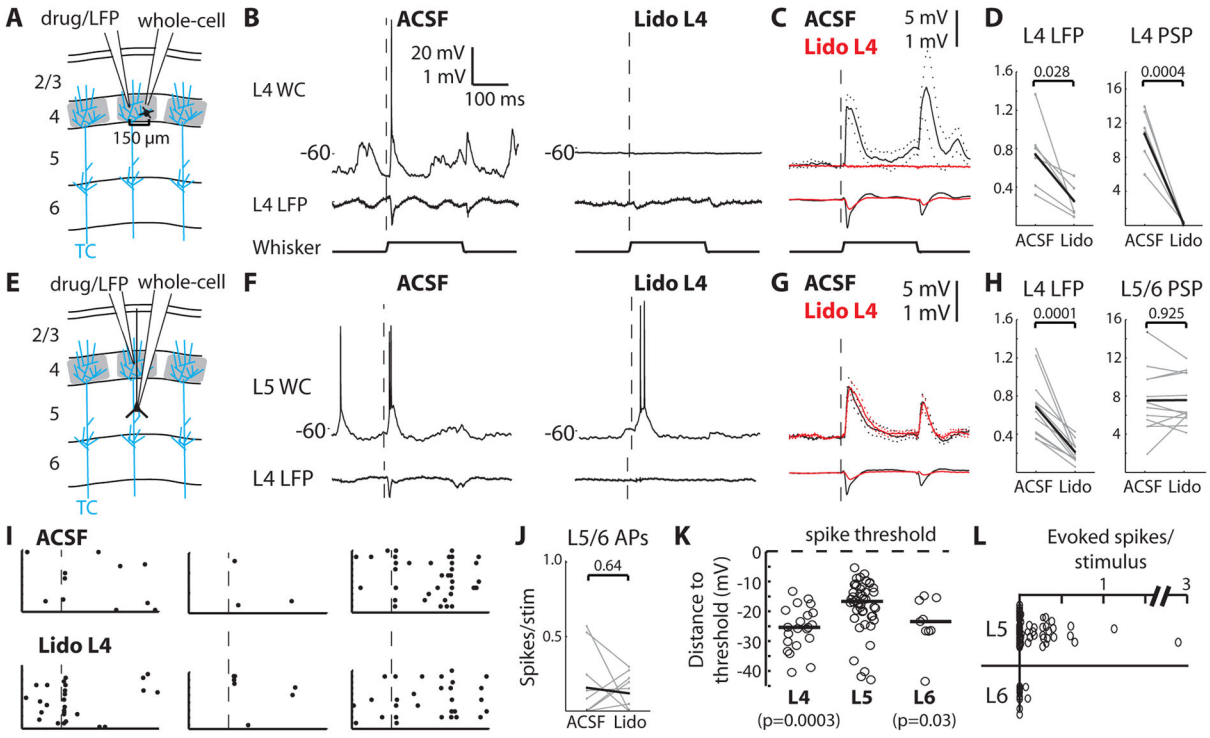

Fig. 3. L5/6 sensory responses do not require L4

(**A**) Whole-cell recordings were made from L4 cells during inactivation of the barrel by lidocaine injection. Blue lines schematically depict single thalamocortical axons, among hundreds per column. (**B**) Simultaneous whole-cell and LFP recordings during injection of ACSF vehicle and lidocaine. Dashed line, onset of whisker deflection in preferred direction. (**C**) Population averages of L4 PSPs (upper) and LFPs (lower). Dashed lines, SEM. (**D**) Summary of responses (in mV). Gray, individual cells; black, means. (**E**) L5/6 recordings were made while L4 was silenced. (**F**), Example L5 whole-cell and L4 LFP traces during ACSF and lidocaine. (**G**) Population averages of L5/6 PSPs (upper) and L4 LFPs (lower). (**H**) Summary plots. (**I**) Rasters of a subset of trials for three example neurons during injection of ACSF (upper) and lidocaine (lower). (**J**) Plots of the baseline-subtracted evoked spikes/stimulus before and after lidocaine injection. (**K**) The relationship between neurons' mean spontaneous membrane potential and spike threshold (L4: n=21; L5: n=46; L6: n=9). Circles, individual cells; lines, medians; p-values, comparison with L5 (Wilcoxon rank-sum). (**L**) Baseline-subtracted evoked spikes/stimulus.

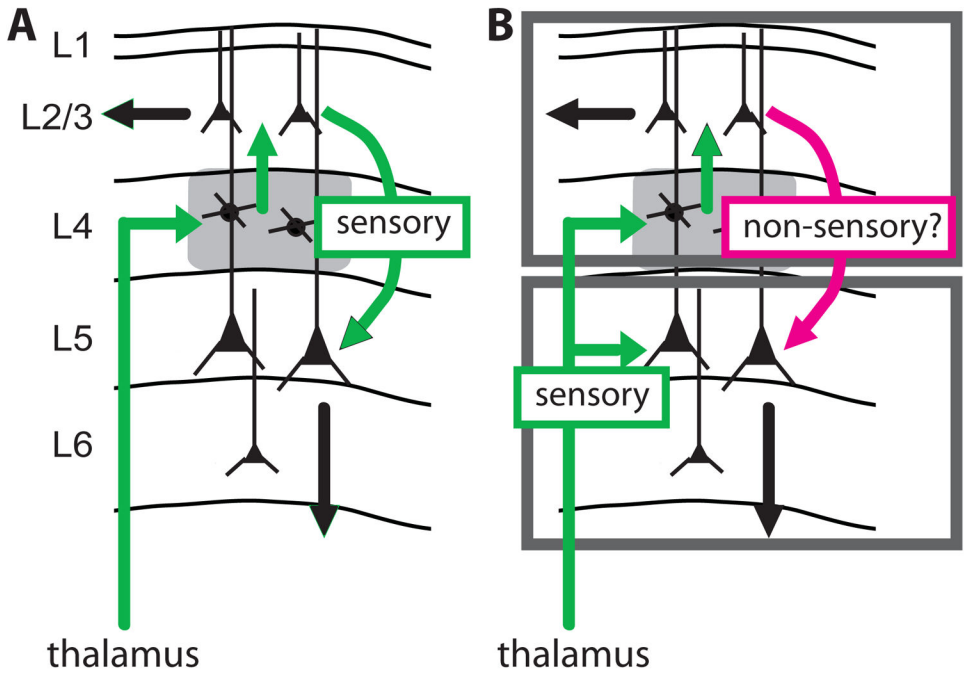

Fig. 4. Schematics of the conventional and proposed models of cortical processing

(**A**) In the conventional serial model, sensory information is transformed as excitation spreads from thalamus, to L4, to L2/3, to L5/6 along the most dense axonal pathways (green). (**B**) In the bistratified model, thalamus copies sensory information to both an upper stratum (L4 and L2/3) and a lower stratum (L5/6), which differs in coding properties and downstream targets.